Rapid Communications

Optimum orientations for octupole deformed nuclei in fusion configurations

Shivani Jain, Manoj K. Sharma, and Raj Kumar*
School of Physics and Materials Science, Thapar Institute of Engineering and Technology, Patiala - 147004, Punjab, India

(Received 29 January 2020; revised manuscript received 29 March 2020; accepted 14 April 2020; published 8 May 2020)

The octupole deformation (β_3) distorts the spherically symmetric or quadrupole deformed (β_2) nuclei into a pear shape. In the present work, the optimum (or uniquely fixed) orientations obtained for the 'elongated' and 'compact' fusion configurations of octupole (β_3) deformed nuclei differ significantly from the ones reported for the quadrupole deformed nuclei. The soft-pear shape nuclei with small β_3 deformations show a maximum deviation of 20° in the elongated and compact configurations, respectively, of oblate and prolate cases, whereas for rigid-pear shape nuclei with strong β_3 deformation, the deviation is of 90°. The optimum orientations obtained are also dependent on '+' and '−' signs of β_3. Thus, octupole deformations significantly modify the optimum orientations for the cold and hot fusion reactions and hence leads to modification of the barrier characteristics. In addition to this, the effects of β_3 have also been observed in the calculation of fusion cross section for the formation of heavy (^{190}Ir*) and superheavy (^{268}Sg*) elements from the octupole-based reactions, i.e., ^{48}Ca(sph.)+^{142}La ($\beta_2 = 0.108$, $\beta_3 = -0.083$) and ^{220}Ra ($\beta_2 = 0.110$, $\beta_3 = -0.125$), respectively.

DOI: 10.1103/PhysRevC.101.051601

The shape of an atomic nucleus in its ground state can be spherical or deformed. The doubly magic nuclei in which neutron and proton shells are completely filled are spherical. As the nucleons (either neutron or proton) are added beyond the magic numbers, it causes a long-range correlation and the nuclear shape starts deviating from spherical configuration. The Coulomb excitation is used as a tool to measure the electric transition probabilities of quadrupole and octupole deformed nuclei [1–4]. The quadrupole deformed nuclei, having axial and reflection symmetry, are the most commonly observed deformed nuclei [5–10]. Unlike quadrupole deformation, it is difficult to observe the effect of the reflection-asymmetry shape in the octupole deformed nuclei. In literature [3,11–16], there are very few experimentally observed octupole nuclei, and limited cases are reported for proton numbers (Z) = 34, 56, 86, and 88, and neutron numbers (N) = 34, 56, 88, 134, and 136. The presence of octupole deformation in a nucleus enhances the nuclear Schiff moments, which in turn, influences the electric dipole moment. Thus, the octupole deformed nuclei are important in the search for permanent electric dipole moments (EDMs) [3,17]. Also, in the nuclear fusion process, the nonzero EDMs in one of the fusing partners (i.e., ^{16}O + ^{144}Ba and ^{224}Ra) show a remarkable impact on the fusion barrier and sub-barrier cross sections [4]. In the present work, we intend to investigate the effect of higher-order multipole deformations (up to β_3) in nuclear fusion reactions (which involve β_3-deformed nuclei either as a projectile or target or both), by obtaining the optimum or uniquely fixed orientations for the 'elongated or cold' and 'compact or hot' fusion configurations of the colliding partners. At these fixed orientations, the significance of higher multipole deformations (up to β_3) can be explored in the synthesis of heavy and superheavy elements.

The shape of a nucleus plays an important role in the nuclear fusion dynamics, and the radius of the deformed nuclei is described in terms of the spherical harmonic multipole expansion [18–21], as given below:

$$R_i(\alpha_i) = R_{0i}\left[1 + \sum_{\substack{i=1,2\\ \lambda=2,3}} \beta_{\lambda i} Y^{(0)}_{\lambda i}(\alpha_i)\right]. \tag{1}$$

Here, $R_{0i}(= 1.28A_i^{1/3} - 0.76 + 0.8A_i^{-1/3})$ represents the radius of the equivalent spherical nucleus. $\beta_{\lambda i}$ is the deformation parameter. $Y^{(0)}_{\lambda i}$ is the normalized spherical harmonic function for axially symmetric shape. Here, $i = 1$ is labeled for projectile and $i = 2$ for target; $\lambda = 2, 3$ stands for quadrupole and octupole deformations, respectively. Note that, in the present work, the values of β_λ for quadrupole ($\beta_{\lambda=2}$) and octupole ($\beta_{\lambda=3}$) deformations are referred from Ref. [21]. As an illustrative case for the graphical representation of deformed nuclei, the deduced β_2- and β_3-deformed shapes of $^{224}_{88}$Ra$_{136}$ from Eq. (1) are presented in Fig. 1 for '+' and '−' signs of β_λ. The quadrupole deformed nuclei, with $\beta_2 < 0$ called oblate—a discus like shape [Fig. 1(a)] and $\beta_2 > 0$ called prolate—a rugby ball like shape [Fig. 1(d)], have symmetry around the axial and reflection axes. On the other hand, the four possible shapes of octupole deformed nuclei (i.e., $\beta_2^-\beta_3^-$, $\beta_2^-\beta_3^+$, $\beta_2^+\beta_3^-$, and $\beta_2^+\beta_3^+$) break symmetry around the reflection axis, as shown in panels (b), (c), (e), and (f) of Fig. 1.

The axial and reflection-symmetric nuclear shapes are found to play a very important role in the synthesis of heavy

*rajkumar@thapar.edu

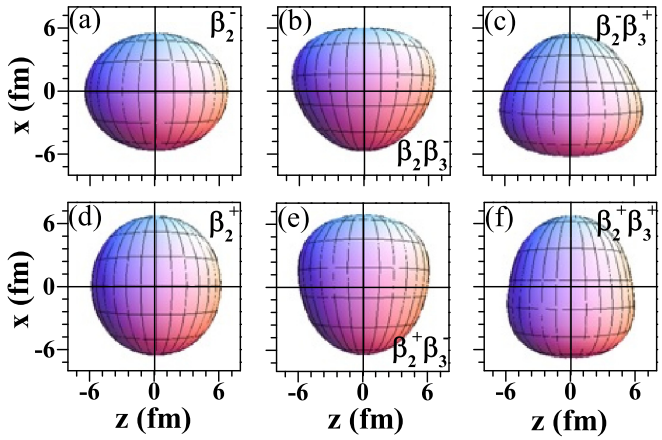

FIG. 1. The graphical representation of quadrupole [(a) β_2^- and (d) β_2^+] and octupole shapes [(b) $\beta_2^-\beta_3^-$, (c) $\beta_2^-\beta_3^+$, (e) $\beta_2^+\beta_3^-$ & (f) $\beta_2^+\beta_3^+$] of $^{224}_{88}$Ra$_{136}$. Here, $\beta_2^{\pm} = \pm 0.143$ and $\beta_3^{\pm} = \pm 0.139$. Horizontal and vertical axes represent the reflection [z (fm)] and axial [x (fm)] axes, respectively.

and superheavy nuclei [22–30]. Further, in the work of Kumar *et al.* [4], the effect of symmetry-breaking shapes has been tested on the fusion barrier distributions. The sensitivity of barrier distributions to octupole deformed targets, such as ^{144}Ba and ^{224}Ra, was tested using ^{16}O-induced reactions and the corresponding impact on the sub-barrier cross sections was analyzed. However, the impact of symmetry-breaking or pear shapes is not understood in the context of fusion dynamics. In the present work, a first step has been taken by analyzing the significance of pear-shape nuclei (belonging to different mass regions of the Periodic Table) on the fusion barriers at optimized orientations. For the synthesis of a compound nucleus either via cold or hot fusion process, the orientation of a deformed nucleus is fixed or optimized in two ways: (i) the elongated configuration which occurs due to the lowest barrier and largest interaction radius between the centers of two nuclei, and (ii) the most-compact configuration that happens at the highest barrier and smallest interaction radius. The steps (i) and (ii) correspond to the 'optimum cold' and 'optimum hot' fusion configurations, respectively. In addition to the above, the effect of octupole deformations, along with their $+/-$ signs, have been analyzed and reported for both the elongated and compact configurations. Note that the nuclei with small and strong octupole deformations are termed as soft- and rigid-pear shaped nuclei, respectively.

The interaction radius (R) and barrier height (V_B) are required to determine the optimum orientations ($\theta_{\rm opt}$). The interaction radius is the distance between the centers of two colliding nuclei, lying in a plane (as shown in Fig. 2), i.e., $R = X_1 + s + X_2 = R_1(\alpha_1)\cos\delta_1 + s + R_2(\alpha_2)\cos\delta_2$. Here, $R_1(\alpha_1)$ and $R_2(\alpha_2)$ are obtained using Eq. (1) of the radius vector. θ_i represents the orientation angle, which rotate in a counterclockwise direction, between the symmetry and collision axes. α_i rotating in the clockwise direction is the angle that the radius vector $R_i(\alpha_i)$ makes with the symmetry axis. The angle δ_i between the radius vector and collision axis in terms of θ_i and α_i is obtained by using the minimization condition [31],

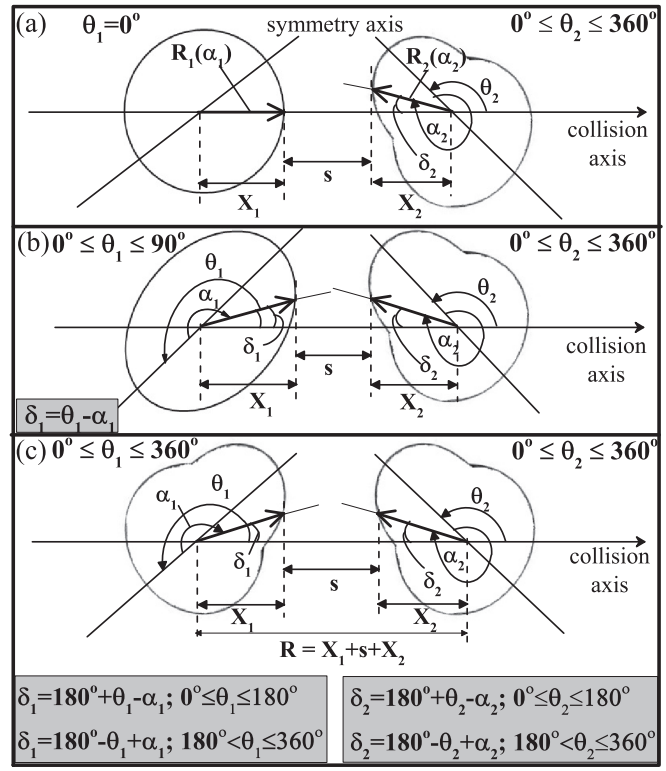

FIG. 2. Schematic configuration of (a) spherical-plus-octupole, (b) quadrupole-plus-octupole, and (c) octupole-plus-octupole axially symmetric deformed and oriented nuclei, lying in the same plane.

which is used to determine the minimum separation distance s between two interacting surfaces. Different iterative methods to fix 's' are available [32,33]. In the proximity potential [see details of Eq. (3)], the shortest distance 's' is taken parallel to the separation distance R along the collision axis. Figure 2 represents the coplanar case of (a) spherical-plus-octupole, (b) quadrupole-plus-octupole, and (c) octupole-plus-octupole deformed nuclei. It is important to note that the quadrupole deformed nuclei have the same configurations at orientations 0° and 180°. However, the pear-shape or octupole nucleus does not have similar configuration at these two extreme angles.

The barrier height (V_B) (used to fix $\theta_{\rm opt}$) is defined as the maximum height attained at a distance where a repulsive Coulomb (V_C) and an attractive nuclear proximity potential (V_N) balance each other. For the higher multipole deformed case, the Coulomb potential is given as [34]

$$V_C = \frac{Z_1 Z_2 e^2}{R} + 3Z_1 Z_2 e^2 \sum_{\lambda=2,3}^{i=1,2} \frac{1}{2\lambda+1} \frac{R_i^{\lambda}(\alpha_i)}{R^{\lambda+1}} Y_{\lambda}^{(0)} \times \left[\beta_{\lambda i} + \frac{4}{7}\beta_{\lambda i}^2 Y_{\lambda}^{(0)}(\theta_i)\right]. \quad (2)$$

The nuclear proximity potential is obtained from the "pocket formula" of Blocki *et al.* [35]. It is a generalized formulation for the deformed and oriented nuclei and given as [31,32,36–39]

$$V_N = 4\pi \bar{R}\gamma b \Phi(s). \quad (3)$$

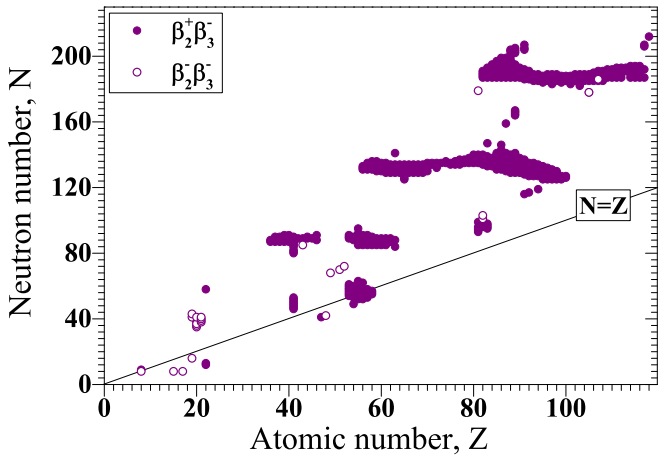

FIG. 3. The octupole deformed nuclei of $\beta_2^+\beta_3^-$ and $\beta_2^-\beta_3^-$ shapes belonging to different mass regions of the Periodic Table. The deformations of more than 700 octupole nuclei are taken from the data table of Möller *et al* [21].

Here, V_N is a product of two terms, one ($4\pi\bar{R}\gamma b$) depends on the shape and geometry (relative orientation) of the colliding nuclei, and another [$\Phi(s)$] depends only on the shortest distance (s) between the two colliding surfaces. The derived proximity potential is valid for all possible colliding partners, irrespective of the choice of minimization conditions used to fix the quantity 's' [31]. The optimum orientations for quadrupole deformed nuclei were obtained by Gupta *et al.* [25]. In the present work, the cold and hot optimum orientations obtained, respectively, for elongated (noncompact) and compact configurations from Eqs. (1) to (3) are exercised for the projectile-target combinations, which involve deformations up to β_3 either in the projectile or target or both the colliding partners. The combinations considered are as follows: spherical+octupole (or octupole+spherical), quadrupole+octupole (or octupole+quadrupole), and octupole+octupole. Here, spherical nuclei are taken as ^{16}O, ^{48}Ca, and ^{208}Pb, quadrupole deformed as ^{48}Ar, ^{62}Fe, and ^{62}Ni, and over 700 octupole deformed nuclei belonging to $8 \leqslant Z \leqslant 118$. The ground-state deformations up to β_3 are taken from the recent Nuclear Data Table of Möller *et al.* [21]. Various β_3-deformed nuclei taken from [21] are shown in Fig. 3 as a function of atomic number (Z). Figure 3 presents the two categories up to β_3-deformed nuclei: (i) the nuclei with weak or small octupole deformation than that of quadrupole, and (ii) the nuclei with strong octupole deformation. In the present work, the optimum orientations determined for the above-mentioned projectile-target combinations are further classified as soft-pear shaped nuclei which have a small effect of β_3, and rigid-pear shape nuclei possessing a strong effect of β_3.

For an illustration, Figs. 4 and 5 present the variation of barrier height (V_B) and interaction radius (R) with respect to the orientation θ_2 of deformed nuclei (as target) of ^{48}Ca+soft-pear (^{110,111,148}La, ^{224,226,232}Rn) and rigid-pear (^{274,276,280}Rn, ^{276,278,280}Ac) nuclear partners. For spherical projectile ^{48}Ca, the corresponding orientation angle θ_1 can be taken as either

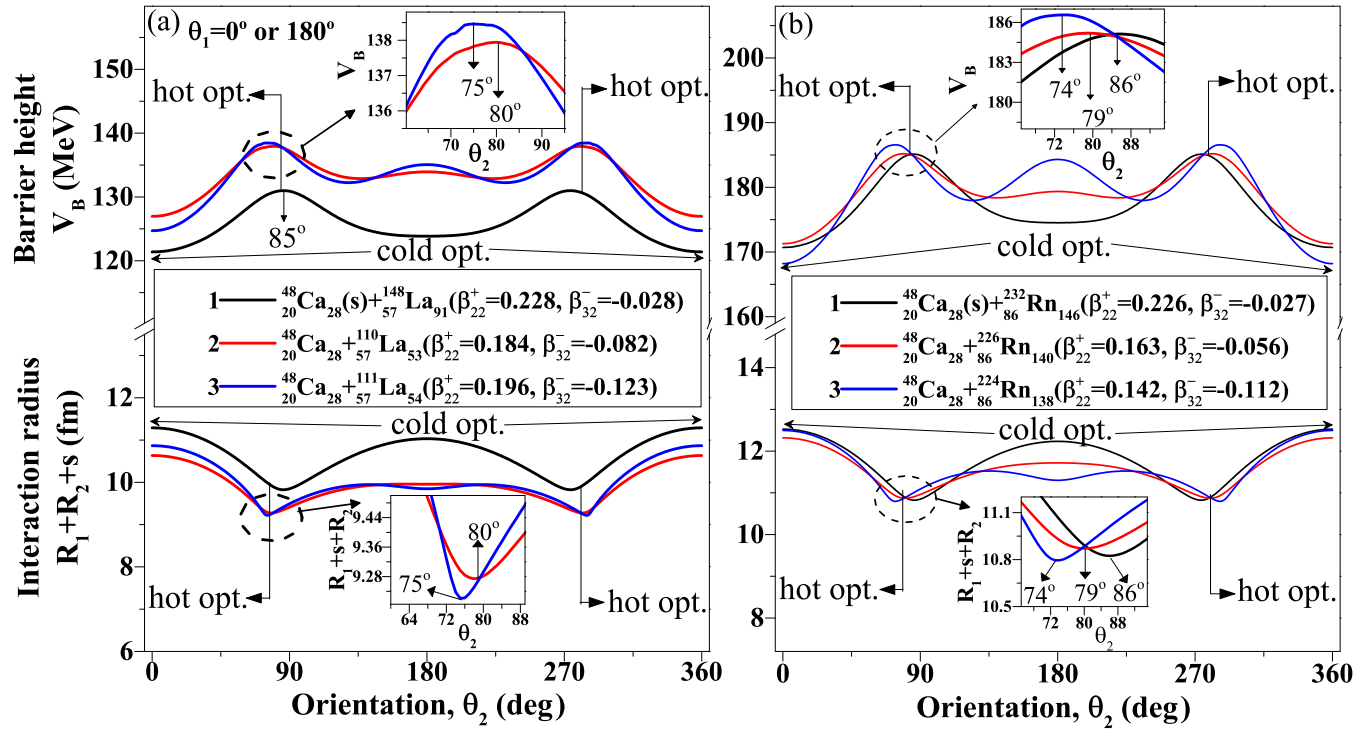

FIG. 4. The variation of barrier height V_B and interaction radius ($R_1 + R_2 + s$) with respect to the orientation (θ_2) of soft-pear shape nuclei in ^{48}Ca (sph) + (a) ^{110,111,148}La and (b) ^{224,226,232}Rn reactions. The difference between the magnitude of β_2 and β_3 is categorized in three categories: (1) $|\beta_2| - |\beta_3| \geqslant 0.2$, (2) $0.1 \leqslant |\beta_2| - |\beta_3| < 0.2$, and (3) $0 < |\beta_2| - |\beta_3| < 0.1$. The arrows signify hot and cold optimum configurations. The insets shows a magnified view of barriers around the hot optimum orientations.

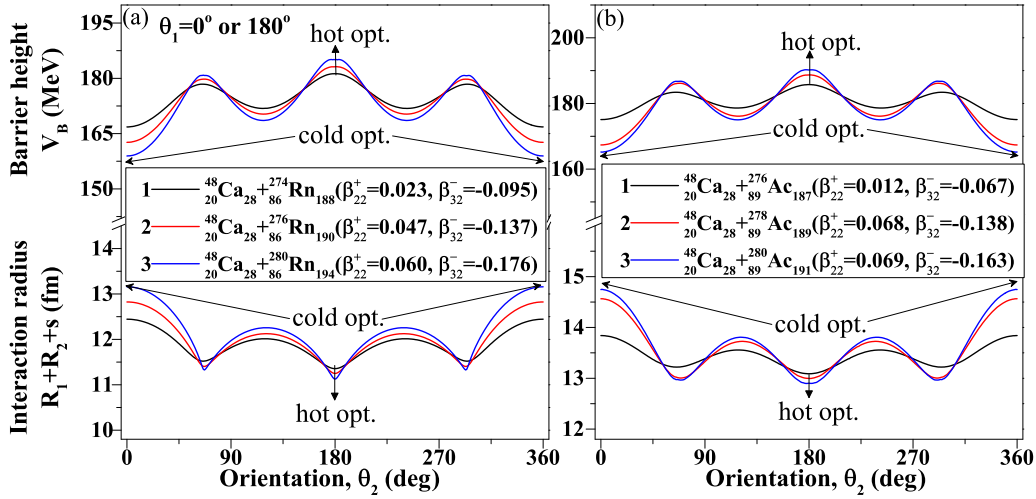

FIG. 5. Same as Fig. 4, but for rigid-pear shape nuclei (as target) in ^{48}Ca (sph) + (a) ^{274,276,280}Rn and (b) ^{276,278,280}Ac reactions.

0° or 180°. In these figures, the elongated configuration of colliding nuclei corresponds to the lowest barrier height and largest interaction radius, which refers to the cold optimum orientation. For the case of compact configuration, the highest barrier and smallest interaction radius stand for the hot optimum orientation. It is worth noting that, in Data Table [21], β_3 deformations are given for $\beta_2^-\beta_3^-$ and $\beta_2^+\beta_3^-$ shapes. The optimum orientations for the rest shapes of octupole nuclei ($\beta_2^-\beta_3^+$ and $\beta_2^+\beta_3^+$) are predicted and reported in Table I by changing the signs of available data for β_3^-. The table presents the optimum orientations ($\theta_2^{\rm opt}$) for spherical-plus-deformed (up to octupole) nuclei. For the case of deformed-plus-deformed combinations, the optimum angles for β_3 deformed cases remain the same as mentioned in Table I. This is evident from orientation conditions for octupole nuclei reported in Fig. 2. In Table I, $\theta_2^{\rm opt}$ for the cold and hot configurations of oblate shape (quadrupole; β_2^-) are 90° and 0° (or 180°), respectively. The spherical-symmetric shapes have the same configurations at 0° and 180°, however, the asymmetric ones have different shapes at these angles. The angular separation between $\theta_2^{\rm opt}|_{\beta_2}$ and $\theta_2^{\rm opt}|_{\beta_3}$ depends on the strength and sign of the octupole deformation. Depending on the magnitude of β_3, $\theta_2^{\rm opt}|_{\beta_3}$ comes with an addition or subtraction of 2°. For the case of the soft-pear shape (i.e., $|\beta_2| > |\beta_3|$), $\theta_2^{\rm opt}$ for the

TABLE I. Optimum orientations for spherical-plus-deformed (up to octupole) nuclei, lying in the same plane, leading to 'cold or elongated' and 'hot or compact' configurations. Note: The optimum orientations obtained for octupole deformed nuclei are developed on the basis of proximity theorem based nuclear potential [see Eq. (3)] in this work, but is valid for any type of nuclear interaction.

			Optimum configuration $\theta_2^{\rm opt}$(degree)	
shape	deformation		'elongated or cold'	'compact or hot'
oblate	β_2^-		90°	0° or 180°
$\lvert\beta_2\rvert > \lvert\beta_3\rvert$	$\beta_2^-\beta_3^-$	$\lvert\beta_2^-\rvert - \lvert\beta_3^-\rvert \geqslant 0.2$	100° ± 2°[a]	180°
		$0.1 \leqslant \lvert\beta_2^-\rvert - \lvert\beta_3^-\rvert < 0.2$	105° ± 2°	180°
		$0 < \lvert\beta_2^-\rvert - \lvert\beta_3^-\rvert < 0.1$	110° ± 2°	180°
soft-pear shape	$\beta_2^-\beta_3^+$	$\lvert\beta_2^-\rvert - \lvert\beta_3^+\rvert \geqslant 0.2$	85° ± 2°	0°
		$0.1 \leqslant \lvert\beta_2^-\rvert - \lvert\beta_3^+\rvert < 0.2$	80° ± 2°	0°
		$0 < \lvert\beta_2^-\rvert - \lvert\beta_3^+\rvert < 0.1$	75° ± 2°	0°
rigid-pear shape	$\beta_2^-\beta_3^-$		0°	180°
$\lvert\beta_2\rvert \leqslant \lvert\beta_3\rvert$	$\beta_2^-\beta_3^+$		180°	0°
prolate	β_2^+		0° or 180°	90°
$\lvert\beta_2\rvert > \lvert\beta_3\rvert$	$\beta_2^+\beta_3^-$	$\lvert\beta_2^+\rvert - \lvert\beta_3^-\rvert \geqslant 0.2$	0°	85° ± 2°
		$0.1 \leqslant \lvert\beta_2^+\rvert - \lvert\beta_3^-\rvert < 0.2$	0°	80° ± 2°
		$0 < \lvert\beta_2^+\rvert - \lvert\beta_3^-\rvert < 0.1$	0°	75° ± 2°
soft-pear shape	$\beta_2^+\beta_3^+$	$\lvert\beta_2^+\rvert - \lvert\beta_3^+\rvert \geqslant 0.2$	180°	100° ± 2°
		$0.1 \leqslant \lvert\beta_2^+\rvert - \lvert\beta_3^+\rvert < 0.2$	180°	105° ± 2°
		$\lvert\beta_2^+\rvert - \lvert\beta_3^+\rvert < 0.1$	180°	110° ± 2°
rigid-pear shape	$\beta_2^+\beta_3^-$		0°	180°
$\lvert\beta_2\rvert \leqslant \lvert\beta_3\rvert$	$\beta_2^+\beta_3^+$		180°	0°

[a]The values of optimum orientations for soft-pear shape nuclei come within the range of $\theta_2^{\rm opt} \pm 2°$.

TABLE II. The calculated fusion cross sections $\sigma_{\rm fus}$ (mb) using Wong formula [34] are given as a function of excitation energy $E^*_{\rm CN}$ [and the corresponding center of mass energy $E_{\rm c.m.}$(MeV)] of an excited compound nucleus ^{268}Sg* [40] formed from the ^{48}Ca (sph)+^{220}Rn ($\beta_2 = 0.110$ and $\beta_3 = -0.125$) reaction.

		Fusion cross sections (σ_{fus}(mb))				
			β_2		β_2, β_3	
$E^*_{\rm CN}$ (MeV)	$E_{\rm c.m.}$ (MeV)	sph	cold	hot	cold	hot
34.67	182.06	14.821	138.132	0.831	472.519	0.129
38.67	186.06	113.204	225.469	49.567	595.856	19.751
43.67	191.06	245.612	395.265	177.279	742.765	144.819
48.67	196.06	371.322	527.931	299.821	882.181	272.095
53.67	201.06	490.780	653.998	416.269	1014.662	393.049
58.67	206.06	604.441	773.947	527.067	1140.714	508.135
63.67	211.06	712.717	888.214	632.615	1260.794	617.767
68.67	216.06	815.981	997.191	733.277	1375.316	722.325
78.67	226.06	1008.805	1200.684	921.244	1589.163	917.566

noncompact configuration of β_2^- changes with a maximum deviation of 20°, whereas the rigid-pear shape ($|\beta_2| < |\beta_3|$) shifts it by 90°. Similar results are observed for the β_2^+ case, but for compact configuration.

It is important to note that the optimum angles change significantly with the magnitude of deformation of soft-pear nuclei. So, the deviations observed in the cold and hot optimum cases for β_2^- and β_2^+, respectively, are categorized in three regions, which show the difference between the magnitude of β_2 and β_3, as (1) $|\beta_2| - |\beta_3| \geqslant 0.2$, (2) $0.1 \leqslant |\beta_2| - |\beta_3| < 0.2$, and (3) $0 < |\beta_2| - |\beta_3| < 0.1$. These regions are exercised for spherical-deformed and deformed-deformed colliding partners, which involve deformations up to β_3 (see Table I and Fig. 2 for details). The considered choices of octupole deformation belong to different mass regions of the Periodic Table.

The present work shows the effect of the sign and magnitude of β_3 deformation for both the compact and noncompact fusion configurations of two colliding nuclei. Unlike quadrupole-deformed nuclei, there are less numbers of experimentally observed octupole nuclei [3,11–16]. That is why the importance of pear-shape nuclei has not been exposed much so far in the field of nuclear reactions. On the basis of our theoretical work, an application of optimized orientations for octupole deformed nuclei is made in the calculation of fusion cross sections ($\sigma_{\rm fus}$) using the Wong formula [34] for the reaction ^{48}Ca(sph)+^{220}Rn($\beta_2 = 0.110$ and $\beta_3 = -0.125$), forming a superheavy compound nucleus ^{268}Sg*, as a function of excitation energies $E^*_{\rm CN}$ (or center of mass energy $E_{\rm c.m.}$). The details are given in Table II. Since the experimental data of this reaction involving the octupole deformed nuclei are not available, so for the sake of comparison, the calculated fusion cross section is compared with the experimental data [40] of the ^{30}Si + ^{238}U reaction, which forms the same compound nucleus, i.e., ^{268}Sg*. It is found that the $\sigma_{\rm fus}$(mb) obtained for the hot configuration of β_3-deformed nuclei (^{220}Rn) seems to be comparable with the experimental data [40]. In addition to this, the calculations have also been done for the formation of a heavy compound nucleus, i.e., ^{190}Ir* formed from the ^{48}Ca(sph) + ^{142}La($\beta_2 = 0.108$ and $\beta_3 = -0.083$) reaction, and the fusion cross sections obtained with the inclusion of β_3 are comparable with the data of the ^{9}Be + ^{181}Ta [41] reaction, which forms the same compound nucleus, i.e., ^{190}Ir*. The results obtained for the synthesis of heavy and superheavy elements from the octupole-based reactions can be verified in future experiments. Also, the importance of optimized orientations for different combinations of colliding partners will be explored in our future work.

The inclusion of soft or rigid-pear shaped deformation of colliding partner shows a significant impact on the fusion barrier and the interaction radius. It is emphasised that an appropriate choice of optimum orientations for the elongated and compact configurations of octupole-deformed nuclei is essential in the analysis of the nuclear fusion dynamics. Such analysis is expected to impart significant relevance in the synthesis and subsequent decay of heavy/superheavy nuclei.

The financial support from DAE, Government of India, sanction no. 58/14/12/2019-BRNS and UGC-DAE Consortium for Scientific Research, File No. UGC-DAE-CSR-KC/CRS/19/NP09/0920 are gratefully acknowledged.

[1] H. Wollersheim *et al.*, Nucl. Phys. A **556**, 261 (1993).
[2] Zhu Sheng-jiang *et al.*, Chin. Phys. Lett. **14**, 569 (1997).
[3] L. P. Gaffney *et al.*, Nature **497**, 199 (2013).
[4] R. Kumar, J. A. Lay, and A. Vitturi, Phys. Rev. C **92**, 054604 (2015).
[5] D. R. Bès and Z. Szymanski, Nucl. Phys. **28**, 42 (1961).
[6] C. W. Towsley *et al.*, Nucl. Phys. A **204**, 574 (1973).
[7] R. W. Ibbotson *et al.*, Phys. Rev. Lett. **80**, 2081 (1998).
[8] E. Nácher *et al.*, Phys. Rev. Lett. **92**, 232501 (2004).
[9] A. Gorgen and W. Korten, J. Phys. G: Nucl. Part. Phys. **43**, 024002 (2016).
[10] N. T. Jarallah, Energy Procedia **157**, 276 (2019).

[11] W. Nazarewicz, P. Olanders, and I. Ragnarsson, Nucl. Phys. A **429**, 269 (1984).
[12] I. Ahmad and P. A. Butler, Annu. Rev. Nucl. Part. Sci. **43**, 71 (1993).
[13] P. A. Butler and W. Nazarewicz, Rev. Mod. Phys. **68**, 349 (1996).
[14] P. A. Butler, J. Phys. G: Nucl. Part. Phys. **43**, 073002 (2016).
[15] B. Bucher *et al.*, Phys. Rev. Lett. **116**, 112503 (2016).
[16] S. J. Zhu *et al.*, Phys. Rev. Lett. **124**, 032501 (2020).
[17] W. Urban *et al.*, Nucl. Phys. A **613**, 107 (1997).
[18] A. Bohr, Mat. Fys. Medd. Dan. Vid. Selsk, **26**, 14 (1952).
[19] A. Bohr and B. R. Mottelson, Mat. Fys. Medd. Dan. Vid. Selsk, **27**, 1 (1953).
[20] D. A. Varshalovich, A. N. Moskalev, and V. K. Khersonskii, *Quantum Theory of Angular Momentum* (World Scientific, Singapore, 1988).
[21] P. Moller *et al.*, At. Data and Nucl. Data Tables **109–110**, 1 (2016).
[22] R. K. Gupta, A. Sandulescu, and W. Greiner, Z. Naturforsch **32a**, 704 (1977).
[23] A. Sandulescu *et al.*, Phys. Rev. Lett. B **60**, 225 (1976).
[24] K. Morita *et al.*, J. Phys. Soc. Japan **73**, 2593 (2004).
[25] R. K. Gupta *et al.*, J. Phys. G: Nucl. Part. Phys. **31**, 631 (2005).
[26] M. Manhas, R. K. Gupta, Q. Li, S. K. Patra, and W. Greiner, Phys. Rev. C **74**, 034603 (2006).
[27] R. K. Gupta, M. Manhas, and W. Greiner, Phys. Rev. C **73**, 054307 (2006).
[28] M. Ismail *et al.*, Can. J. Phys. **92**, 1411 (2014).
[29] S. Chopra, Hemdeep, P. Kaushal, and R. K. Gupta, Phys. Rev. C **98**, 041603(R) (2018).
[30] G. Kaur, K. Hagino, and N. Rowley, Phys. Rev. C **97**, 064606 (2018).
[31] R. K. Gupta, N. Singh, and M. Manhas, Phys. Rev. C **70**, 034608 (2004).
[32] M. Seiwert *et al.*, Phys. Rev. C **29**, 477 (1984).
[33] V. Yu. Denisov and N. A. Pilipenko, Phys. Rev. C **76**, 014602 (2007).
[34] C. Y. Wong, Phys. Rev. Lett. **31**, 766 (1973).
[35] J. Blocki *et al.*, Ann. Phys. (NY) **105**, 427 (1977).
[36] N. Malhotra and R. K. Gupta, Phys. Rev. C **31**, 1179 (1985).
[37] M. Manhas and R. K. Gupta, Phys. Rev. C **72**, 024606 (2005).
[38] D. Jain, R. Kumar, and M. K. Sharma, Nucl. Phys. A **915**, 106 (2013).
[39] G. Kaur, K. Sandhu, and M. K. Sharma, Nucl. Phys. A **971**, 95 (2018).
[40] K. Nishio, H. Ikezoe, I. Nishinaka, S. Mitsuoka, K. Hirose, T. Ohtsuki, Y. Watanabe, Y. Aritomo, and S. Hofmann, Phys. Rev. C **82**, 044604 (2010).
[41] N. T. Zhang *et al.*, Phys. Rev. C **90**, 024621 (2014).